Ulmeanu, M., Petkov, P., Ursescu, D., Jipa, F., Harniman, R., Brousseau, E., & Ashfold, M. N. R. (2016). Substrate surface patterning by optical near field modulation around colloidal particles immersed in a liquid. *Optics Express*, *24*(24), 27340-27351. https://doi.org/10.1364/OE.24.027340

Substrate surface patterning by optical near field modulation around colloidal particles immersed in a liquid

M. ULMEANU,[1, 5,*], P. PETKOV,[2] D. URSESCU,[3] F. JIPA,[4] R. HARNIMAN,[1] E. BROUSSEAU,[2] AND M. N. R. ASHFOLD[1]

[1]*School of Chemistry, University of Bristol, Bristol BS8 1TS, UK*
[2]*Cardiff School of Engineering, Cardiff University, Cardiff CF24 3AA, UK*
[3]*Extreme Light Infrastructure Nuclear Physics (ELI-NP)/Horia Hulubei National Institute for R and D in Physics and Nuclear Engineering (IFIN-HH), Bucharest 077125 Romania*
[4]*National Institute for Laser, Plasma and Radiation Physics, Bucharest 077125 Romania*
**magdalena.ulmeanu@bristol.ac.uk*

Abstract: Optical near field enhancements in the vicinity of particles illuminated by laser light are increasingly recognized as a powerful tool for nanopatterning applications, but achieving sub-wavelength details from the near-field distribution remains a challenge. Here we present a quantitative analysis of the spatial modulation of the near optical fields generated using single 8 ps, 355 nm (and 532 nm) laser pulses around individual colloidal particles and small close packed arrays of such particles on silicon substrates. The analysis is presented for particles in air and, for the first time, when immersed in a range of liquid media. Immersion in a liquid allows detailed exploration of the effects on the near field of changing not just the magnitude but also the sign of the refractive index difference between the particle and the host medium. The level of agreement between the results of ray tracing and Mie scattering simulations, and the experimentally observed patterns on solid surfaces, should encourage further modelling, predictions and demonstrations of the rich palette of sub-wavelength surface profiles that can be achieved using colloidal particles immersed in liquids.

OCIS codes: (220.0220) Optical design and fabrication; (290.0290) Scattering; (140.0140) Lasers and laser optics.

References and links

1. Y. Kawata, C. Egami, O. Nakamura, O. Sugihara, N. Okamoto, M. Tsuchimori, O. Watanabe, "Non-optically probing near-field microscopy," Opt. Commun. **161**, 6-12 (1999).
2. H. J. Muenzer, M. Mosbacher, M. Bertsch, J. Zimmermann, P. Leiderer, J. Boneberg, Local field enhancement effects for nanostructuring of surfaces," J. Microscopy **202**, 129 -135 (2001).
3. P. Kuehler, D. Puerto, M. Mosbacher, P. Leiderer, F. J. Abajo, J. Siegel, J. Solis, "Femtosecond-resolved ablation dynamics of Si in the near field of a small dielectric particle," Beilstein J. Nanotechnol. **4**, 501-509 (2013).
4. Z. Chen, A. Taflove, V. Backman,"Photonic nanojet enhancement of backscattering of light by nanoparticles: a potential novel visible-light ultramicroscopy technique," Opt. Express **12**, 1214 -1220 (2004).
5. P. Kuehler, F. J. Garcia de Abajo, J. Solis, M. Mosbacher, P. Leiderer, C. N. Afonso, J. Siegel, "Imprinting the optical near field of microstructures with nanometer resolution," Small **5**, 1825-1829 (2009).
6. M. Ulmeanu, P. Petkov, D. Ursescu, V. A. Maraloiu, F. Jipa, E. Brousseau, M. N. R. Ashfold, "Pattern formation on silicon by laser-initiated liquid-assisted colloidal lithography," Nanotechnology **26**, 455303 (2015).
7. E. D. Palik, *Handbook of Optical Constants of Solids* (Academic 1988).

[5] Married name M. Stanton

8. I. H. Malitson, "Interspecimen comparison of the refractive index of fused silica," J. Opt. Soc. Am. **55**, 1205 - 1209 (1965).
9. G. Mie, "Beiträge zur Optik trüber Medien, speziell kolloidaler Metallösungen," Ann. Phys. Lpz. **330**, 377 – 445 (1908).
10. https://optics.synopsys.com/rsoft/application-gallery/mie-scattering.html
11. Z. B. Wang, W. Guo, A. Pena, D. Whitehead, B. S. Lukyanchuk, L. Lin, Z. Liu, Y. Zhou, M. H. Hong, "Laser micro/nano fabrication in glass with tunable-focus particle lens array," Opt. Express **16**, 19706 -19711 (2008).
12. K. Piglmayer, R. Denk, D. Bauerle, "Laser-induced surface patterning by means of microspheres," Appl. Phys. Lett. **80**, 4693 - 4695 (2002).
13. M. Y. Shen, C. H. Crouch, J. E. Carey, E. Mazur, "Femtosecond laser-induced formation of submicrometer spikes on silicon in water,"Appl. Phys. Lett. **85**, 5694 – 5696 (2004).
14. K. Moutzouris, M. Papamichael, S. C. Betsis, I. Stavrakas, G. Hloupis, D. Triantis, "Refractive, dispersive and thermo-optic properties of twelve organic solvents in the visible and near infrared," Appl. Phys. B **116**, 617 – 622 (2014).
15. I. Martin-Fabiani, J. Siegel, S. Riedel, J. Boneberg, T. A. Ezquerra, A. Nogales, "Nanostructuring thin polymer films with optical near fields," ACS Applied Materials & Interfaces **5**, 11402 -11408 (2013).

1. Introduction

The quest to fabricate ever more complex nanopatterns and extended periodic arrays on solid surfaces using low cost yet effective lithographic methods has stimulated huge interest in near field (NF) optical effects, *i.e*. in phenomena associated with non-propagating and highly localized electromagnetic fields and their interaction with matter. Optical NF effects can be generated in the vicinity of metal or dielectric nanoparticles, where the localization of electromagnetic energy leads to an increase in the incident field intensity [1]. The NF enhancements caused by dielectric spherical colloidal particles in air have been used to create isolated holes in silicon substrates [2, 3]. The NF intensity distribution in such NF-laser ablation (NF-LA) studies is revealed by localized ablation of the substrate, in the form of an isolated crater, at the peak of the field distribution. Single shot, 'parallelized' processing of larger surface areas has been realized in air, using a close packed monolayer array of such particles as a mask. Previous studies have shown the emergence of sub-wavelength photonic beams ("nanojets") from the reverse of a dielectric microsphere illuminated by light of wavelength λ [4]. These non-evanescent and non-resonant beams, which can be generated using a wide range of sphere sizes, are characterized by a narrow lateral size (of order $\sim\lambda/3$) and can propagate over distances $d > \lambda$ provided that the ratio of the refractive indices of the sphere and the background medium is < 2:1. Envisioned applications of such photonic nanojets include sub-diffraction resolution nanopatterning, ultra-high-density optical data storage, optical trapping, and waveguiding. Studies employing a photosensitive $Ge_2Sb_5Te_5$ film have afforded a more detailed view of the complex 2-D NF intensity distribution beneath a scattering colloidal particle [5]. Rather than requiring ablation, this latter study allowed visualization of a much wider distribution of NF intensities by analyzing the spatial variation of different phases induced at the substrate surface. These authors also reported simulations of the electric field distribution at the substrate plane that recognized near field effects from propagated focused light and scattering from the sphere and reflection from the substrate.

The present work expands and generalizes such analyses by considering NF effects induced by light interacting with individual colloidal particles (or small arrays of such particles) on a substrate surface immersed in a liquid – rather than in air. Our preliminary demonstration of the single pulse, laser induced liquid assisted colloidal (LILAC) lithography technique [6] revealed complex patterning of silicon substrates. The patterning was regarded as an imprint of the spatial intensity modulation formed by diffraction of the laser pulse by the colloidal particle(s). The detailed surface topography was shown to depend upon the relative indices of refraction of the colloidal particle (n_{colloid}) and the liquid (n_{liquid}), *i.e*. on whether the incident light converges ($n_{\text{colloid}} > n_{\text{liquid}}$) or diverges ($n_{\text{colloid}} < n_{\text{liquid}}$) on interaction with the particle.

However, that study provided little quantitative detail concerning the spatial modulation of the field around each colloidal particle or how the surface topography was influenced by the particle size or the refractive index difference $\Delta n = (n_{colloid} - n_{liquid})$.

Here, we report an in-depth study of the surface patterning achieved using single colloidal particles and/or well separated monolayer clusters of such particles. The surface patterns resulting from one shot irradiation of such clusters are shown to reflect the spatial modulation of the NFs generated by each constituent particle. The study provides the first quantitative analysis of the spatial modulation of the NF as a result of localized focusing/defocusing of the propagating light and interference between the incident and scattered light around individual colloidal particles, on silicon substrates immersed in different liquid media, following irradiation with a single picosecond (ps) UV laser pulse. In the narrative that follows, these near field 'focusing' and 'scattering' contributions are discussed as NF-F and NF-S effects. Parameters varied in the present study include the particle material, its radius, R (in the range 350 nm $\leq R \leq$ 5 μm) and the liquid medium, which allows us to explore the evolution of the NF-induced patterning with changes in Δn. Topographical changes to the silicon substrate have been analyzed by scanning electron microscopy (SEM) and atomic force microscopy (AFM). The study illustrates the promise of LILAC lithography as a route for patterning and texturing Si surfaces on the nanoscale and for providing fundamental insights into short laser pulse – matter interactions in the NF.

2. Experimental method

One of the harmonics of a diode pumped Nd:YVO_4 laser system, normally the third harmonic of wavelength, λ_0 = 355 nm, with a full width half maximum (FWHM) pulse duration of 8 ps and a repetition rate of 10 kHz, was used to effect spatially localised, single pulse ablation of a silicon (Si) surface. The scan pattern was designed to ensure exposure of a series of equally spaced areas of diameter 25 μm (in air) on the substrate, each of which was subjected to a single shot of focused (Gaussian spatial beam profile) radiation. The laser beam was controlled using WaveRunner software (Nutfield Technology) and a galvo-scanner combined with a telecentric lens with focusing distance f = 103 mm. Powers, P, used in the present work spanned the range $5 < P < 50$ mW, which translate into incident fluences, F, at the substrate surface in the range $0.28 < F < 2.8$ J cm^{-2}. The incident light was circularly polarized by use of a quarter-waveplate. The Si substrates were cut from n-type Si wafers (Crystal GmbH) and pre-treated in an oxygen plasma (Femto Diener, 80 W power, 0.5 mbar O_2 pressure) for 10 min to remove contaminants and render the surface hydrophilic. We assume bulk values for the optical constants of these Si substrates (i.e. n = 5.61 and k = 3.014 at λ = 355 nm) [7]. Two families of particles were used in the present work: silica particles with radius R = 1.5 μm or 350 nm (Bangs Laboratories), and polystyrene particles with R = 5 μm (Sigma Aldrich). The respective manufacturers quote $n_{colloid}$ = 1.44 (silica) and $n_{colloid}$ = 1.59 (polystyrene), both measured at λ = 589 nm. For the wavelength of most current interest, λ = 355 nm, $n_{colloid}$ (silica) = 1.476 [7] and $n_{colloid}$ (polystyrene) = 1.649 [8].

A number of low-dimensional arrangements of these colloidal particles on Si substrates have been investigated. The colloid particles were deposited in isolation, or as 2, 3 or 4 particle clusters, by spin coating a low particle concentration solution onto the substrate. The colloid coated Si substrate was then completely immersed in the liquid of interest (volume ~1 cm^3) in an open trough (of dimension 25 × 25 × 20 mm^3) mounted on a motorised 2-(X, Y-) axis translation stage. Single shot laser irradiation in the chosen liquid usually resulted in particle removal but, if that did not occur (*e.g.* when irradiating at low F), any remaining particles were removed using scotch tape in order to access the imprinted NF surface patterns. Sample characterization involved use of optical microscopy, scanning electron microscopy (JEOL IT300 SEM), atomic force microscopy (Bruker Multimode AFM) and high-resolution (HR) transmission electron microscopy (JEOL JEM ARM200F TEM).

3. Results and discussion

The present study explores characteristics of LILAC lithographic processing under two limiting cases – when each spherical particle can be considered as an isolated entity, or when these particles are part of a small cluster (when more complex cross-scattering is observed). In air or in liquid, the patterns produced when a laser pulse is incident on such isolated or groups of colloidal particles can be pictured in terms of contributions from: a) ablation rings, caused by NF-F effects if the peak intensities exceed the threshold intensity for ablating the substrate, and b) finer structures with characteristic minima and maxima, that depend on interference between the incoming laser beam, light scattered by the particle and light reflected at the substrate surface [3]. In what follows, we explore how the distributions of ablation rings depend on Δn and R, how the topographies and the periodicity of the minima and maxima vary with R, and how the complex topographies in areas covered by small arrays of close packed particles arise during LILAC lithographic processing.

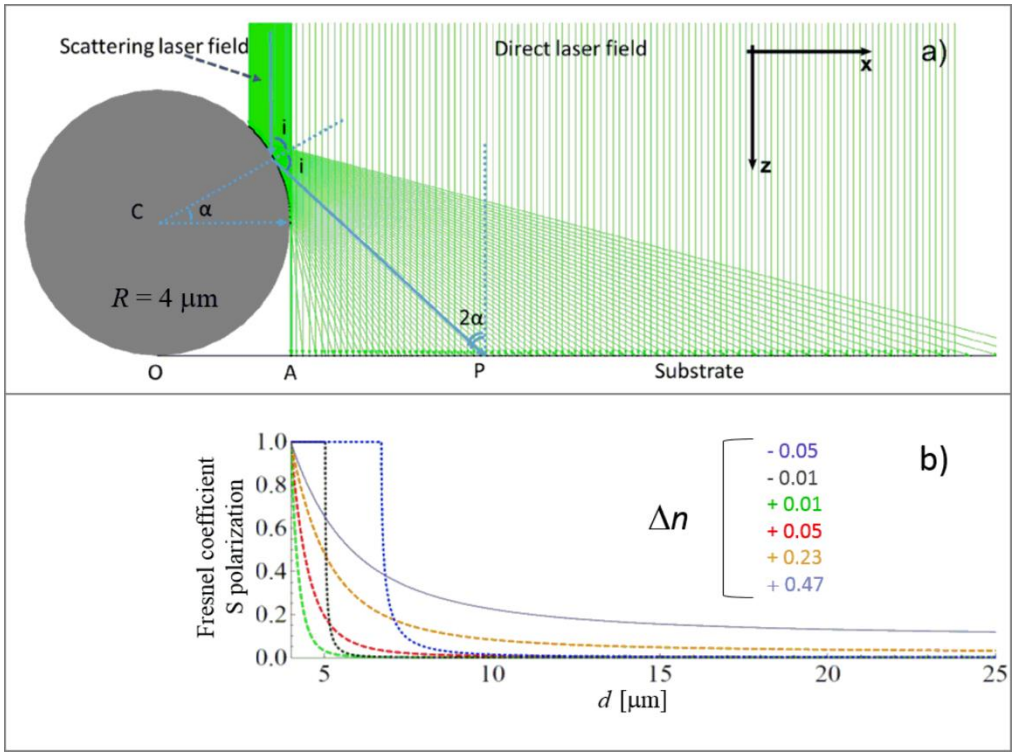

Fig. 1. (a) Diagram illustrating the interference between rays that are directly incident on a substrate and those that strike it after reflection from the surface of an R = 4 μm spherical particle with $n_{colloid}$ = 1.47. The light propagates in the +Z direction and is linearly polarized along X. (b) Fresnel reflection coefficient for rays scattered to different points on the substrate in air (n_{air} = 1.00, Δn = 0.47) and in liquids with different n_{liquid} (and thus different Δn combinations), plotted as a function of distance d beyond the sphere radius.

Prior to presenting the experimental data it is useful to sketch the problem using the simplified ray-tracing model of the experimental configuration as illustrated in Fig. 1. The ray-tracing approximation provides a rationale for the pattern imprinted on the substrate at radii greater than that of the spherical particle in terms of interference between light directly incident on the substrate and light scattered from the particle (i.e. NF-S effects). This interference

pattern is determined by the angle θ between the direct and scattered rays at the substrate surface and the wavelength λ of the light in the medium in which the particle is immersed according to eq. (1)

$$d_f = \lambda / sin\theta \quad (1)$$

where d_f is the separation between successive fringes.

We define θ by parametrizing the position of the ray striking the sphere as in Fig. 1(a), where α defines the angle between the radius to the interaction point and the horizontal axis through C, the centre of the sphere, in the plane of incidence. Given a collimated incident beam propagating along the substrate surface normal, the angle θ between the two interfering waves on the substrate is given by eq. (2)

$$\theta = 2\alpha \quad (2)$$

Equations (1) and (2) allow estimation of the fringe separations at different positions on the substrate. Clearly, the d_f will decrease with increasing radial distance d, defined as the distance from the edge of the particle (point A) onwards, i.e. larger θ. Only rays incident on the sphere at $\alpha \lesssim 45°$ will scatter to the substrate surface. For such rays, eqs. (1) and (2) imply a limiting fringe spacing comparable to their wavelength, i.e. $d_f \gtrsim \lambda$. We also note that any such fringes formed by scattering from a given particle will be more tightly spaced when the particle is immersed in a liquid with refractive index $n_{\text{liquid}} > 1$ (as in the LILAC technique) than when in air ($n_{\text{air}} = 1.00$), given that the effective wavelength of the incident radiation in the liquid λ_{liquid} is smaller (by a factor of n_{liquid}) than in vacuum or air.

A fuller understanding of the NF-S interference pattern on the substrate requires not just the fringe positions but also the intensity distribution of the scattered radiation. This depends on the incident field multiplied by the Fresnel reflection coefficients in the medium of interest for rays with $\alpha < 45^0$ (or, in terms of angle of incidence on the particle, $i = (90 - \alpha°)$). Figure 1(b) shows the Fresnel coefficients calculated for s-polarised radiation scattering from a spherical particle with R = 4 μm and $n_{\text{colloid}} = 1.47$ in air ($\Delta n = 0.47$) and in several model liquids giving Δn values in the range 0.25 to – 0.05, as a function of radial position on the substrate. The calculated reflectivity is highest at large i, corresponding to small α and small d, when the scattered radiation is incident on the substrate in (or close to) the NF region. The Fresnel coefficient decreases with increasing d in all cases, but the rate of decline is most gradual when the particle is in air and increases with decreasing (positive) Δn. In the case that $n_{\text{liquid}} > n_{\text{colloid}}$ (negative Δn), total internal reflection (*i.e.* the Fresnel coefficient is unity) is observed for incidence angles $i \geq i_{total}$, where i_{total} is described in the Eq. 3:

$$i_{total} = \arcsin(n_{\text{colloid}}/n_{\text{liquid}}) \quad (3)$$

Rays striking the sphere at incident angles i just below i_{total} see an almost perfect mirror, are reflected onto the substrate in the immediate vicinity of the sphere, interfere with the direct wave and build fringes with amplitudes approaching twice that of the incident field (i.e. to field intensities almost 4-times higher than that from just the directly incident radiation). Once $i << i_{total}$, however, the reflection coefficient again drops rapidly, the amplitude of the scattered radiation reaching the substrate becomes small and contributes little to the intensity pattern on the substrate at larger radius.

Such a ray tracing model serves to highlight the much richer variety of scattering behavior and surface patterning enabled by use of different liquid media (i.e. by tuning Δn with the LILAC lithography method) rather than simply irradiating in air, but is not able to predict diffraction effects due to the presence of the sphere boundary. FullWAVE 9.1 software (RSoft Design) is a finite-difference time-domain FDTD-based Maxwell equation solver that can be used to directly simulate Mie scattering and produces results in excellent comparison

with Mie theory [9, 10]. Thus we have also applied this model in an effort to characterize the field distribution attributable to NF-F effects.

The simulation model in this case comprises a single sphere irradiated with λ_0 = 355 nm laser light that, as in Fig. 1, is linearly polarized along *X* and propagates in the +*Z* direction. The grey scale images shown in Figs. 2(a) and 2(b) depict the calculated electric field intensity distributions, $|E^2|$, perpendicular to the *XZ* plane for a particle with R = 1.5 μm immersed in a liquid such that Δn is, respectively, positive and negative. Since $R >> \lambda$, these distributions are dominated by Mie scattering effects. Panels ($a_{1\text{-}3}$) and ($b_{1\text{-}3}$) show the localized regions of field enhancement in the *XY* plane at the *Z* position that would correspond to the particle-substrate contact (in the event that a substrate was present), for three different R and Δn combinations. The reported intensities are referenced to unity – the value that would apply in the absence of the colloidal particle. Note that the declines at extreme $|X|$ in these panels are an artefact caused by the attenuating boundary used in the simulations.

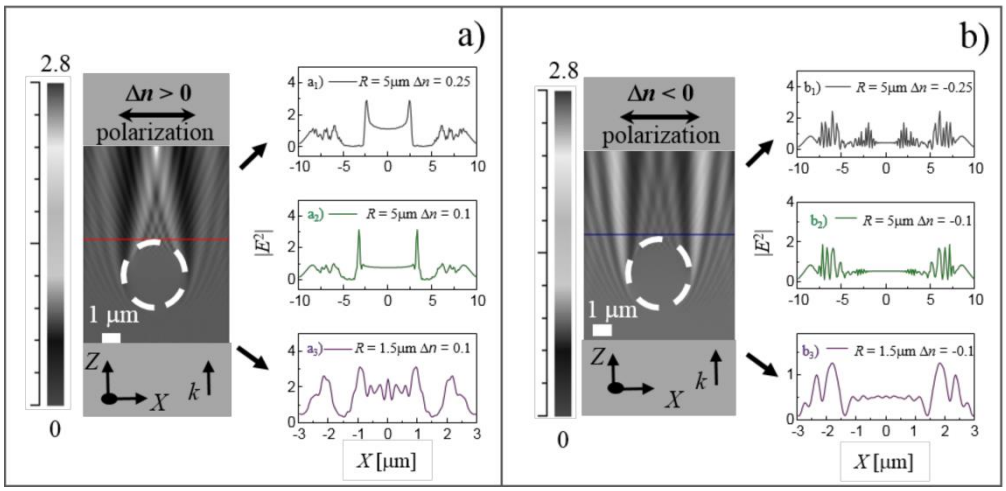

Fig. 2. False grey scale plots showing the $|E^2|$ distributions returned by FDTD simulations for a single sphere with radius R = 1.5 μm and $n_{colloid}$ = 1.44 immersed in a liquid medium such that a) $\Delta n > 0$ and b) $\Delta n < 0$. The dashed white circle shows the position of the colloidal particle. The incident radiation (λ_0 = 355 nm) is linearly polarized (along *X*) and propagates with wavevector *k* in the +*Z*-direction. The grey scale used is shown at the far left and indicates the intensity immediately behind the particle (i.e. at the position a substrate surface would occupy) relative to that of the incident wave (defined as 1.0). The panels to the right of each grey scale plot show cuts through calculated $|E^2|$ distributions along *X*, in the *XY* plane, at the point $Z = R$, for different combinations of R and Δn: (a_1) R = 5 μm, Δn = +0.25; (a_2) R = 5 μm, Δn = +0.1; (a_3) R = 1.5 μm, Δn = +0.1; (b_1) R = 5 μm, Δn = – 0.25; (b_2) R = 5 μm, Δn = – 0.1; (b_3) R = 1.5 μm, Δn = – 0.1.

The $|E^2|$ vs *X* profiles clearly illustrate how the colloidal particle acts as a convergent ($\Delta n > 0$) or divergent ($\Delta n < 0$) lens [6], and how immersing the particle in different liquid media provides a route to extending the focal length of the NF-F region [11]. Compared with NF-LA in air, where ablation is localised to the region of contact between the particle and the substrate (*i.e.* where $|E^2|$ is maximal [12]) the LILAC lithography technique allows the user to 'tune' the region of maximal $|E^2|$ on the substrate surface. The present FDTD modelling confirms that the light intensity incident on a surface beneath a particle immersed in a liquid chosen so that $\Delta n > 0$ is increased by the presence of the particle, to an extent that scales with Δn. As Figs. 2(a_1)–2(a_3) show, the calculated $|E^2|$ distribution for small positive Δn shows two (or more) prominent maxima, but the distribution gradually evolves to a single maximum under the geometric centre of the particle in the limit of large Δn – consistent with the NF-LA in air

results. The reverse trend is seen with negative Δn, see Figs. 2(b_1)–2(b_3). In this case, the presence of the particle reduces the intensity of laser light incident on the substrate area it eclipses but provides some boost to $|E^2|$ at X values greater than R.

The FDTD modelling also shows that, for given $|\Delta n|$, the full width half maxima (FWHM) values for the regions of intensity enhancement narrow with increasing R, irrespective of whether the colloidal particle is acting as a convergent or divergent lens. This can be seen by comparing the $|E^2|$ vs X cuts shown in Figs. 2(a_2) and 2(a_3) or in Figs. 2(b_2) and 2(b_3); the predicted FWHM of the regions of enhanced $|E^2|$ with the R = 5 μm particle in Fig. 2(a_2), for example, is ~ 45 nm. Multiple regions of enhanced $|E^2|$ are predicted in the case that $\Delta n < 0$ (*i.e*. the particle is acting as a divergent lens), each with a very narrow FWHM value. We note that the $|E^2|$ enhancements (factors of 2-3) predicted by these simulations under LILAC relevant conditions are much smaller than the factor of ~ 30 predicted by similar calculations for NF-LA in air using an R = 0.85 μm particle [2], but also reiterate the greater variety of surface patterns achievable with the LILAC lithography method.

3.1 Surface patterning in air

Armed with this information, we now present examples of the topographic patterning of Si surfaces induced by single λ_0 = 355 nm pulsed laser irradiation of colloidal particles in air or immersed in different liquids. The data presented in Figs. 3 and 4 are for samples processed in air, wherein Δn is always positive. Figure 3 shows illustrative SEM images for two different particle sizes and refractive indices, as detailed in the caption.

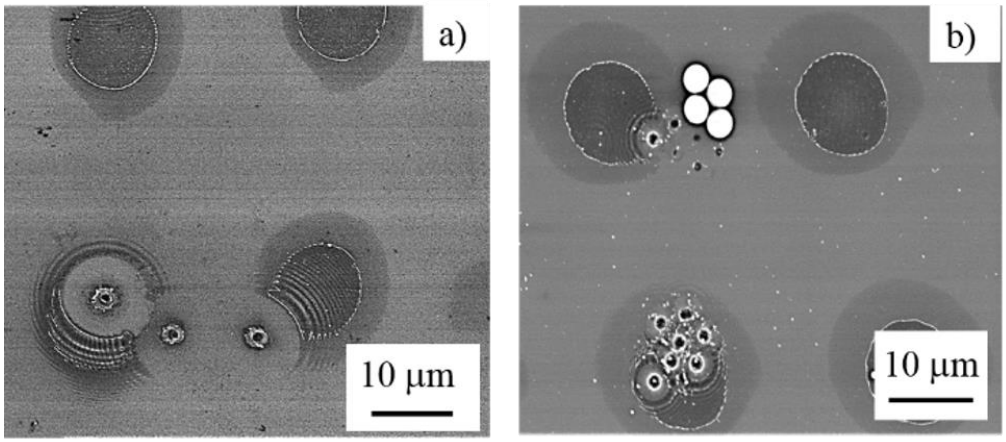

Fig. 3. SEM images illustrating patterns achieved on Si substrates by illuminating the translating sample surface with a train of equi-spaced laser pulses. The respective areas contained (a) one or (b) more than one colloidal particles with respective particle sizes and refractive indices as follows: a) R = 5 μm, $n_{colloid}$ = 1.64 and b) R = 1.5 μm, $n_{colloid}$ = 1.47 with, in both cases, n_{liquid} = 1.00 (air). The centre of the substrate area eclipsed by the particle of interest prior to irradiation is determined by the hole created by NF-F (i.e. NF-LA) effects, the larger darkened areas are the surface regions subjected to greater than some threshold incident fluence, and the white discs near the top of (b) are a cluster of four particles that were not removed in the LILAC processing.

The darkened areas evident in these SEM images were each irradiated with just a single laser pulse, with a Gaussian spatial profile, incident along the surface normal. The translation of the substrate ensures that the irradiated areas are equally spaced, but the centre of the Gaussian intensity profile (revealed as the larger darker regions) will not generally coincide with the geometric centre of the projection of any one spherical particle onto the substrate

surface. We caution that, for this reason, F values quoted in the rest of this study necessarily represent an upper limit to the fluence experienced by the colloidal particle(s) of interest. The observed patterns arise from NF-F and NF-S effects, which can be understood by recalling the scattering, i.e. Fig. 1, and the FDTD, i.e. Fig. 2, model outputs. Several localized ablation craters are clearly evident (as dark spots) in the images shown in Fig. 3. These arise from NF-F induced ablation at positions directly under the centre of particles that were removed by the laser irradiation process, and are reminiscent of the craters reported in previous NF-LA studies in air [2]. NF-S effects manifest themselves as a series of concentric rings outside the area eclipsed by the original particle, as shown in greater detail in Fig. 4(a). AFM analysis confirms that the light/dark rings correspond to, respectively, maxima/minima in the local topography. The interference of the NF-S rings from two close packed colloidal particles gives a regular 3D nanotexture to the silicon surface, as shown in Fig. 4(b). These NF-S rings, which resemble ripples on the surface of a liquid [13], are only evident in regions where the reflectivity of the Si surface has been modified during the interaction with the single laser pulse, i.e. the darker regions in the SEM images in Fig. 3. The distance from the centre of the NF-LA induced crater to the first ring depends on the size of the colloidal particle and the additional NF-S rings fade in intensity and become progressively more closely spaced as the radial distance increases in a manner that is entirely consistent with that predicted by Eqs. (1) and (2).

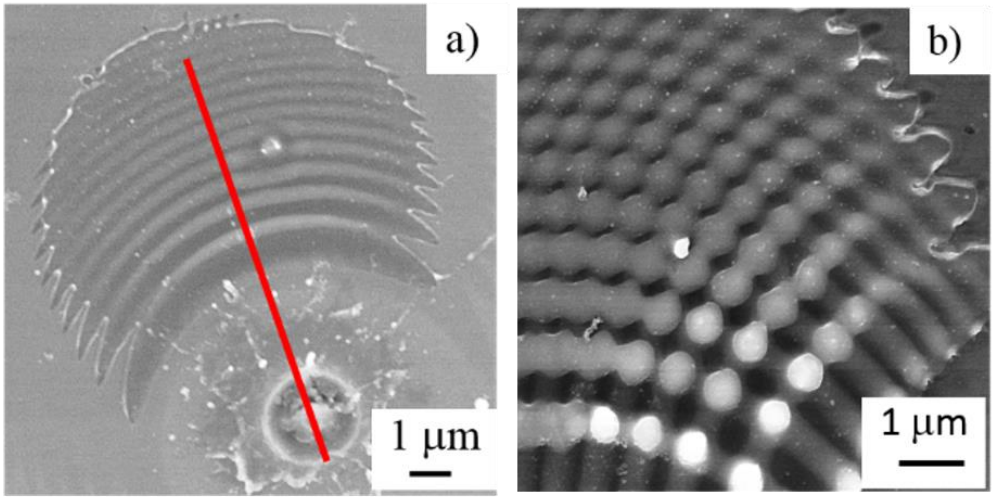

Fig. 4. SEM images showing the NF-LA and NF-S patterns formed on a Si surface by single pulse λ_0 = 355 nm laser irradiation of: a) one and b) two close packed colloidal particles with R = 5 μm, $n_{colloid}$ = 1.64, in air (n_{liquid} = 1.00). The red line shows the radius along which the cross-sectional profile shown in Fig. 7(a) was measured.

3.2 Surface patterning under a liquid

The remaining examples highlight facets of LILAC processing of a Si substrate using spherical colloidal particles immersed in a liquid. The patterns shown in Fig. 5 were formed using silica particles (R = 1.5 μm, $n_{colloid}$ = 1.47) in toluene. The refractive index of toluene at λ_0 = 355 nm is n_{liquid} = 1.52, derived by extrapolating the value at λ = 589 nm using the dispersion equations reported in the literature [14]. Thus $\Delta n < 0$ in these examples and the NF-F patterns will appear as an ablation ring rather than the localized ablation crater seen in the case of NF-LA in air. The radius of this ablation ring (relative to the centre of the colloidal particle) can be tuned by changing the size of the colloidal particle or the magnitude of Δn [6]. The NF-S

rings are again confined to areas outside the radius of the colloidal particle but, as we show below, the topographies can be very different from those formed in air.

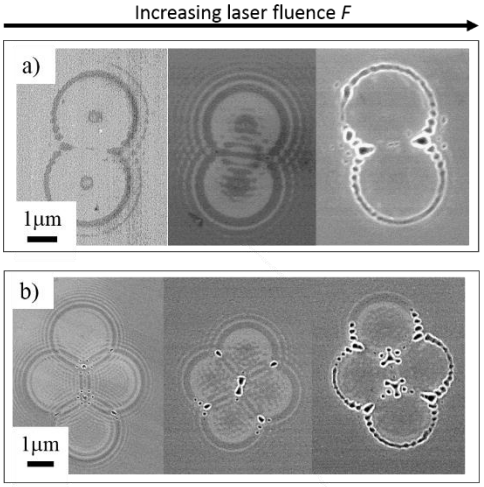

Fig. 5. SEM images of patterns formed by LILAC processing of a Si substrate surface immersed in toluene (n_{liquid} = 1.52) with a single 355 nm laser pulse. Each exposed area contained a close-packed cluster comprising (a) 2 and (b) 4 colloidal particles with R = 1.5 μm and $n_{colloid}$ = 1.47, which were exposed to, respectively, F = 0.85 J cm^{-2} (left), 1.3 J cm^{-2}(centre) and 2.2 J cm^{-2} (right).

The SEM images in Figs. 5(a) and 5(b) reveal alternant dark and bright rings corresponding to regions of the surface that have been exposed to, respectively, enhanced and reduced incident intensities. The LILAC pattern formed at low F reveals parts of the Si substrate that are seemingly untouched. Additional concentric rings are evident in the case of particles exposed to higher F. The periodicity of these surface patterns is tighter than when ablating in air, recall Figs. 3 and 4, reflecting the reduced effective wavelength of the light ($\lambda = \lambda_0/n_{liquid}$) and the ring pattern is less extensive than that formed by ablating in air, reflecting the faster drop in the scattered field intensity with increasing R, recall Fig. 1.

The tilt-view AFM images shown in Figs. 6(a) and 6(b) allow assessment of the topographical changes of the Si surface formed by irradiating close packed clusters of three R = 1.5 μm, $n_{colloid}$ = 1.47 colloid particles immersed in toluene (n_{liquid} = 1.52) at two different incident fluences, F = 0.85 J cm^{-2} (a) and 2.2 J cm^{-2} (b). In both images, the innermost ring is attributable to NF-F induced ablation, and the extended wrinkle patterns are the result of interference between the incident field and light scattered by the colloidal particles (i.e. NF-S effects). The innerrmost ablation ring reflects the calculated $|E^2|$ distribution, which shows two (or more) obvious maxima under the conditions prevailing in LILAC lithography (recall Fig. 2) rather than a single maximum under the geometric centre of the particle in the limit of large, positive Δn (as found for NF-LA in air). The radial separation between the NF-LA ring and the first of the rings attributable to NF-S effects is ~450 nm and the subsequent inter-ring separations clearly decrease with increasing R. The annular region between each NF-S ring appears unmodified in patterns formed at low F, but the surface topography is visibly different when processed at higher F. Focusing on the substrate exposed to higher F (image (b)), the NF-LA ring is a shallow 'moat' of depth only ~ 12 nm and width ~ 150 nm. Much deeper, higher aspect ratio craters are formed in regions where the NF-F and/or NF-S rings associated with different particles overlap: for example, the craters formed in regions where an NF-F and NF-S field overlap are ~ 35 nm deep and ~ 215 nm wide, while the central crater formed from the overlap of three separate NF-F fields is ~ 40 nm deep and ~ 300 nm wide.

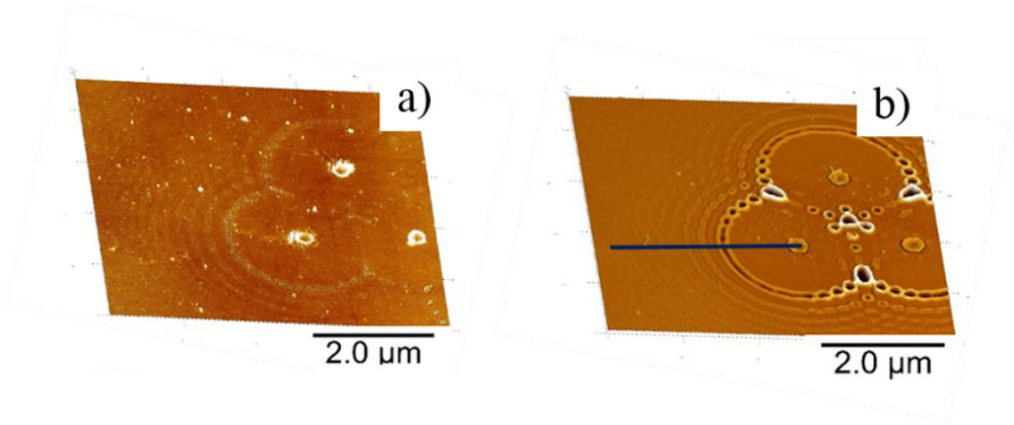

Fig. 6. Tilt view AFM images of the NF patterns imprinted on a Si substrate by LILAC lithographic processing using a single 355 nm laser pulse and close-packed arrays of three colloidal particles with R = 1.5 µm and $n_{colloid}$ = 1.47 in toluene (n_{liquid} = 1.52) and an incident fluence (a) F = 0.8 J cm^{-2} and (b) F = 2.2 J cm^{-2}. The blue line in Fig. 6(b) shows the radius along which the cross-sectional profile shown in Fig. 7(b) was measured.

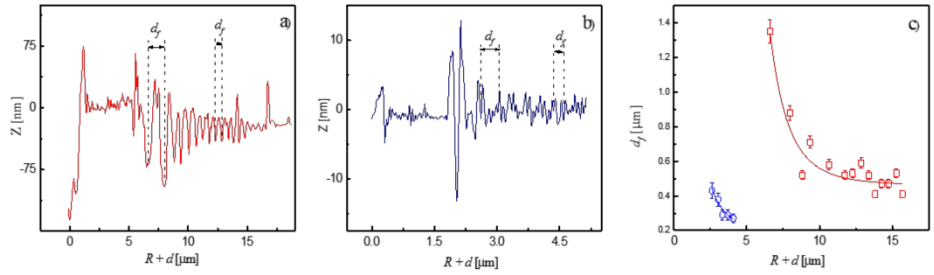

Fig. 7. Cross-sectional AFM traces illustrating different topographical profiles that arise when the particle acts as (a) a converging lens (R = 5 µm, $n_{colloid}$ = 1.64 in air (n_{liquid} = 1), i.e. $\Delta n > 0$, along the red line in Fig. 4(a), and (b) a diverging lens (R = 1.5 µm, $n_{colloid}$ = 1.47 in toluene (n_{liquid} = 1.52), i.e. $\Delta n < 0$, along the blue line in Fig. 6(b). (c) Illustration of the decreasing separation d_f between the NF-S rings arising using different R and Δn combinations, plotted as a function of distance from the particle centre, i.e. (R + d). The period of the NF-S rings is smaller in liquid than in air, and tends to the predicted λ/n_{liquid} value as the far field is approached.

Figures 7a) and 7b) show AFM cross-section profiles from the centre of the projection of the spherical particle onto the Si substrate for two different colloid particle/'liquid' combinations. The trace in Fig. 7(a) is along the radius shown in red in Fig. 4(a), i.e. for an R = 5 µm, $n_{colloid}$ = 1.64 particle in air (n_{liquid} = 1), which acts as a converging lens ($\Delta n > 0$). Figure 7(b), in contrast, shows the pattern achieved with an R = 1.5 µm, $n_{colloid}$ = 1.47 particle in toluene (n_{liquid} = 1.52) i.e. along the radius shown in blue in Fig. 6(b), which is representative of the topography formed with a diverging lens ($\Delta n < 0$). Careful inspection of Fig. 7(a) reveals ablated rings due to NF-S effects on a background that itself shows evidence of having been lightly ablated (i.e. even the 'maxima' between the rings in this $\Delta n > 0$ case are slightly below the level of the virgin substrate surface). In the latter ($\Delta n < 0$) case, the NF-S rings appear as much fainter surface modulations, i.e. the light fringes in Fig. 6(b). These contrasting behaviors can be understood by recalling the model outputs presented in Fig. 1. NF-S effects rely on the interference between the direct and scattered fields at the substrate surface. For any incident E, the amplitude of the radiation field scattered by the particle (and thus the magni-

tude of the interference cross-term) is largest when $d \sim 0$ and declines with increasing d but at a rate that decreases with increasing Δn. This accords with the topographic modulation evident in Fig. 7(a); the interference in the case that $\Delta n = 0.47$ is sufficient to ablate material at the d values corresponding to several NF-S rings. For the case of divergent lens ($\Delta n < 0$), however, Fig. 1 shows the amplitude of the scattered radiation falling much more steeply with increasing d. Given that the incident E-field alone was insufficient to cause material ablation in this particular experiment, the increased intensity in regions of constructive interference with the scattered radiation from a colloidal particle is only sufficient to cause a localized phase change (e.g. melting) – as evidenced by the NF-S ring patterns in Fig. 6 – rather than discernible ablation.

The topographic profiles shown in Fig. 7(a) allow a further point of contact with the model predictions. As Fig. 7(b) shows, the separations between successive fringes d_f – ablation minima in Fig. 7a), topographic maxima in Fig. 7(b) – declines with increasing d, consistent with Eqs. (1) and (2), and tend to the expected value of $\lambda_0/n_{\text{liquid}}$ at large d (i.e. 355 nm in the case of ablation in air, and ~235 nm for the ablation in toluene). All of these data serve to highlight the potential of the LILAC lithographic technique for extending single-pulse surface nanopatterning capabilities far beyond that already demonstrated in air [15].

Our final example illustrates the sensitivity of the NF distribution to changes in the colloidal particle size and the laser wavelength λ_0. Figure 8 shows three tilt-view SEM images of Si surfaces patterned using the LILAC technique and close-packed arrays of colloidal spheres with $n_{\text{colloid}} = 1.47$ immersed in carbon tetrachloride ($n_{\text{liquid}} = 1.48$). The samples shown in Figs. 8(a) and 8(b) were formed using spheres with $R = 1.5$ μm and 350 nm, respectively, and a laser wavelength, $\lambda_0 = 355$ nm. The same $R = 350$ nm spheres were used when generating the patterned surface in Fig. 8(c) but, in this case, $\lambda_0 = 532$ nm. These serve to illustrate further the potential flexibility of the patterning achievable with LILAC lithography. NF-F effects (i.e. NF-LA) dominate the patterns formed with small spheres. i.e. $R \sim \lambda_0/n_{\text{liquid}}$, as in Fig. 8(c), but decreasing λ_0, as in Fig. 8(b), and/or increasing R, as in Fig. 8(a), increases the opportunity for constructive overlap between the NF-F and NF-S fields, resulting in progressively more localized, high-aspect ratio craters.

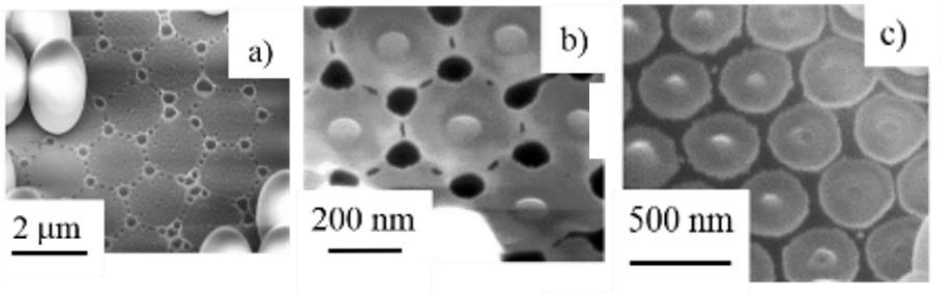

Fig. 8. Tilt view SEM images showing the Si surface patterns achieved by single shot LILAC processing with a single layer of colloidal particles ($n_{\text{colloid}} = 1.47$), immersed in carbon tetrachloride ($n_{\text{liquid}} = 1.48$). The respective particle sizes and irradiation wavelengths were: (a) $R = 1.5$ μm, $\lambda_0 = 355$ nm, (b) $R = 350$ nm, $\lambda_0 = 355$ nm, and (c) $R = 350$ nm, $\lambda_0 = 532$ nm.

4. Conclusion

The surface patterning achieved with the LILAC technique is shown to originate from a combination of near field and scattering field (and their mutual interference) arising from individual colloidal particles. Patterns formed by single pulse irradiation of Si substrates supporting single particles, isolated clusters of particles and more extended close packed particle arrays

in air and in different liquid media have all been investigated by SEM and AFM. Guided by complementary ray-tracing and FDTD numerical simulations, such analysis allows us to distinguish contributions from near field focusing/defocusing and from scattering effects, and to understand their respective sensitivities to the refractive index difference (Δn) between the colloidal particle and the background medium. The overlap of NF-F and NF-S fields offers a route to forming variable aspect ratio holes with sub-wavelength FWHM cross-sections. The degree of consistency between the surface patterning demonstrated in this study and the modelled electric field distributions should encourage further opportunities and applications involving the LILAC technique. The work also suggests that patterns formed on a substrate by LILAC processing could be used to characterize the refractive index (or the distribution of refractive indices) of a monodisperse ensemble of scattering particles (e.g. cells) or the size distribution within an ensemble of particles (e.g. gas bubbles) with a common refractive index.

Funding

M.U. is grateful for the award of a Marie Curie International Intra-European Fellowship, Research Executive Agency (FP7-PEOPLE-2013-IEF-625403). D.U. is supported by Extreme Light Infrastructure Nuclear Physics (ELI-NP) Phase II, a project co-financed by the Romanian Government and European Union through the European Regional Development Fund. F.J. is supported by the National Authority for Research and Innovation in the frame of the Nucleus program (contract 4N/2016).